Proceedings of International Conference on Heat Exchanger Fouling and Cleaning VIII - 2009 (Peer-reviewed)
June 14-19, 2009, Schladming, Austria
Editors: H. Müller-Steinhagen, M.R. Malayeri and A.P. Watkinson

Published online
www.heatexchanger-fouling.com

# FLUID DYNAMIC GAUGING APPLIED TO ANNULAR TEST APPARATUSES FOR FOULING AND CLEANING

**T. Gu[1*], F. Albert[2], W. Augustin[2], Y.M.J. Chew[1], W.R. Paterson[1], S. Scholl[2], I. Sheikh[1], K. Wang[1], D.I. Wilson[1]**

[1]Department of Chemical Engineering and Biotechnology, University of Cambridge, New Museums Site, Pembroke Street, Cambridge CB2 3RA, UK, Tel: (44) 01223 330144, Fax: (0044) 01223 334796
[2]Technical University of Braunschweig, Institute for Chemical and Thermal Process Engineering
Langer Kamp 7, 38106 Braunschweig, Germany, Tel: (0049) 531 391-2789 Fax: (0049) 531 391 2792
[*]Corresponding author: tg277@cam.ac.uk

## ABSTRACT

Fluid dynamic gauging (FDG) is a non-contact technique for measuring the thickness and strength of fouling layers immersed in liquid in situ. These studies demonstrate its application to an annular geometry across a range of possible flow conditions, from stagnant to turbulent flow regimes (Reynolds ~ 29 000). The results were not affected significantly by the surface under study being heated, indicating that the technique is suitable for measuring deposit thicknesses in situ during fouling experiments. Computational fluid dynamics simulations, which afford detailed information about the flow patterns and shear stresses imposed on the surface, showed good agreement with experimental data for tests in the laminar regime. A short study of whey protein fouling confirmed the feasibility of using FDG to monitor fouling layers.

## INTRODUCTION

Fouling in heat transfer systems is often unavoidable and reduces energy efficiency and plant operability. Mitigation of fouling and effective cleaning strategies both require understanding of the mechanisms involved in deposition and cleaning. Experimental studies are often required to develop this knowledge. One of the key properties affecting cleaning and removal is the thickness and strength of a fouling deposit, which will change over time and is difficult to quantify. Tuladhar *et al*. (2000) developed the technique of fluid dynamic gauging (FDG) for measuring the thickness of fouling deposits immersed in a liquid environment *in situ* and non-invasively. A schematic of the gauge is presented in Fig. 1: the gauge works as a siphon, whereby a pressure difference between the fluid near the substrate surface and the discharge end of the gauge causes liquid to flow into the nozzle. This discharge flow rate, $m$, is measured and the pressure difference calculated. For a given pressure driving force the flow rate is uniquely related to the distance between the nozzle and the surface, *i.e.* the clearance, $h$. Measurements of $m$ allow $h$ to be calculated, and changes in $h$ can be related to the increase (fouling) or decrease (cleaning) of deposit thickness. The main limitation is that the foulant should be sufficiently stiff that it does not change shape during the measurement. The gauge is operated so that its internal flow is always in the laminar regime.

Tuladhar *et al.* developed the technique of 'quasi-static FDG' to study surface layers on flat surfaces, where the bulk liquid was still, apart from the flow generated by the gauging action. This mode has been successfully applied to fouling and cleaning studies on a diverse range of foulant materials and surfaces. Tuladhar *et al*. (2003) and later Hooper *et al*. (2006) demonstrated that FDG can be applied to monitor the growth and removal of whey protein fouling layers on a flat surface exposed to a imposed bulk flow of liquid in a duct of square cross section (termed 'flow FDG') with a precision of ± 10 μm. Recently, Gu *et al*. (2009a) described the application of dynamic gauging to an inner convex surface of an annular duct. They reported results for quasi-static conditions and where the flow in the annulus was in the turbulent regime. This study extends that work to the laminar and transitional annular flow regimes.

This paper presents experimental FDG results from two concentric *annular* devices, this geometry being a popular configuration for heat transfer and fouling experiments (e.g. the HTRI fouling probe). An FDG device was incorporated to these to extend the types of data which can be generated in such investigations. The first device, at Cambridge (labelled apparatus 1), is geometrically similar to an annular test cell under construction at Imperial College London for tests on crude oil fouling, with outer and inner annulus diameters of 35 mm and 21 mm, respectively. Experiments were conducted in laminar, transitional and turbulent flows (corresponding to annulus Reynolds numbers in the range $90 < Re_{annulus} < 32\,000$) and in quasi-static flow (no bulk flow in the annulus). The second device, labelled apparatus 2, located at Braunschweig, features outer and inner annular diameters of 30 mm and 12 mm, respectively. This unit is used for studies of fouling on heated surfaces and is employed here in a whey protein fouling test.

Alongside experimental studies, computational fluid dynamics (CFD) simulations were performed to estimate the shear stresses imposed on the surface being gauged. Knowledge of the shear stress, and thereby the rheology of the deposit, is important for both fouling and cleaning studies. CFD models were constructed to calculate the

velocity fields and the shear stress acting on surface by the action of the gauging flow. The governing Navier-Stokes and continuity equations of the steady-state, laminar, Newtonian and incompressible flow were solved numerically using the finite element method (FEM), and the results compared with the experimental data.

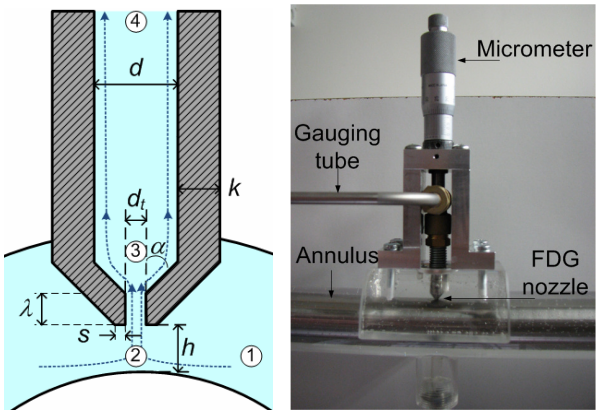


Fig. 1 Schematic (left) and picture (right) of fluid dynamic gauge (FDG) in an annular geometry. The schematic shows dimensional parameters of the gauge. Numbers 1 to 4 signify various locations in the system.

## APPARATUS

### Apparatus 1

Apparatus 1 was employed for the quasi-static, laminar, transitional and turbulent flow tests using water at 20 ℃ as the test fluid. The length of the annulus is 1 m and its hydraulic diameter, $D_h$, 14 mm. The concentric annulus was held vertically (Fig. 2). The outer tube was constructed from acrylic for visualisation purposes, while a length of 316 stainless steel rod was used for the inner tube, to ensure a stiff surface; early trials using an acrylic inner tube experienced significant vibration which impaired the measurements. Concentricity was maintained using three metal locating pins at the inlet and outlet of the annulus. To ensure fully developed flow the gauge is located 750 mm from the entry ($54D_h$). For fully developed turbulent flow, $10D_h$ is generally deemed sufficient (Bennett *et al.,* 2007). However, statistically fully developed turbulent flow, with no significant variation in axial flow characteristics, may be achieved only after a length of $50D_h$ (Baker *et al.*, 1999). Water passes upwards through the annulus. Three different flowmeters, R1, R2 and R3, were used for laminar, transitional and turbulent flows. The mean velocity through each were: R1, 0.0068 – 0.055 m/s ($60 < Re_{annulus} < 800$); R2, 0.04 - 0.15 m/s ($600 < Re_{annulus} < 2100$); and R3, 0.26 – 2.06 m/s ($3\,580 < Re_{annulus} < 29\,000$), where $Re_{annulus}$ was defined in terms of $D_h$.

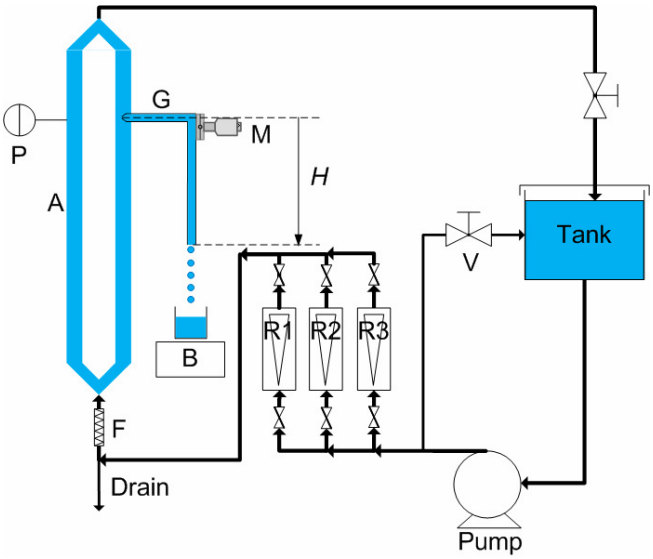


Fig. 2 Schematic of apparatus 1: A – annular test section; B – electronic balance; V – flow control valve; F - filter; G – gauging tube; *H* – hydrostatic head. M – micrometer; P – gauge pressure sensor; R- flowmeter.

The gauge was operated with the bulk flow rate through the annulus maintained constant. Two pressures were responsible for driving the gauging flow. The first is the suction pressure caused by the hydrostatic head, *H*, which was maintained constant at 405 mm (equivalent to 3970 Pa). The second is the static gauge pressure, $p_s$, associated with the annular flow. This latter pressure was measured using a pressure sensor (accuracy ± 34 Pa), located 750 mm from the inlet of the annulus, diametrically opposite the gauging nozzle. The measured $p_s$ values ranged from –1100 Pa (at $Re_{annulus} = 90$) to 34 300 Pa (at $Re_{annulus} = 29\,000$).

### Apparatus 2

Apparatus 2, shown in Fig. 3, tested the behaviour of the gauge in a slightly different annular geometry, and where the surface was heated. The dimensions of the annulus were: i.d. 12 mm, o.d. 30 mm and length 430 mm. The heated section was 406 mm long. The inner heating rod was made of 316 stainless steel. The outer pipe was acrylic and the annulus was again located vertical with fluid flowing upwards. Temperatures were measured at the inlet and outlet of the test section, and at the heated wall. Constant bulk temperature (defined as the arithmetic mean of the inlet and outlet temperature of the test section) was maintained using a plate heat exchanger (cooler).

De-ionised water was used for calibration of the gauge and for constant heat flux experiments. 5 wt% whey protein concentrate (WPC) solution was employed for the fouling experiments, at a bulk temperature of 54 °C.

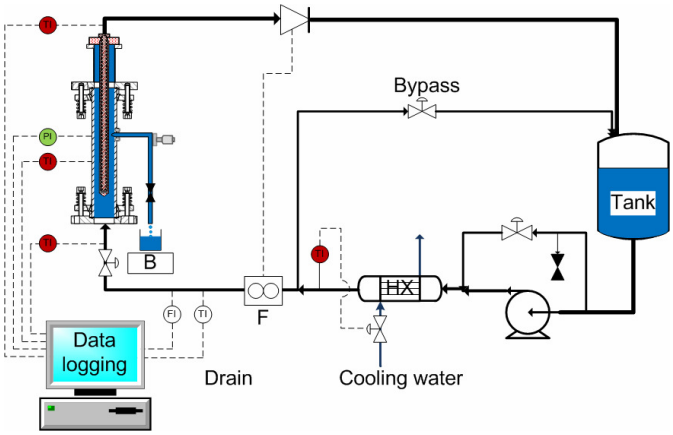


Fig. 3 Schematic of apparatus 2: A – annular test section; B – electronic balance; F – flow indicator; G – gauging tube; HX – heat exchanger.

**Gauging nozzle**

The gauges used in the apparatuses differed slightly. Both were fabricated from 316 stainless steel. The gauge in apparatus 1 had dimensions (Fig. 1): $d_t$ = 1 mm, $d$ = 4 mm, $k$ = 2 mm, $s$ = 0.5 mm, $\alpha$ = 45° and $\lambda$ = 1.5 mm. Gauge 2 dimensions were: $d_t$ = 1 mm, $d$ = 4 mm, $k$ = 1 mm, $s$ = 0.12 mm, $\alpha$ = 30° and $\lambda$ = 1.5 mm.

The gauge can be moved backwards and forwards horizontally, normal to the inner tube, through a seal, using a micrometer. These two operating modes are referred to as *nozzle retreating* and *nozzle advancing*, respectively. The micrometer reads the distance between the surface of the inner rod and the tip of the nozzle, $h$. The discharge gauging flow was measured using an electronic balance (accuracy ± 0.05 g).

The performance of the nozzle was quantified using the nozzle discharge coefficient, $C_d$, which accounts for the energy losses due to the flow around the nozzle entrance. $C_d$ is defined as the ratio of the actual to ideal mass flow rate through the nozzle:

$$C_d = \frac{m_{actual}}{m_{ideal}} = \frac{m}{\frac{\pi d_t^2}{4}\sqrt{2\rho\Delta p_{13}}} \qquad (1)$$

where

$$\Delta p_{13} = \Delta p_{14} - \Delta p_{34} = \rho g H + p_s - \frac{128\mu m l_{eff}}{\pi d^4 \rho} \qquad (2)$$

Subscripts 1, 3 and 4 refer to various locations in the system shown in Figs. 1 and 4. The static pressure (near the nozzle), $p_s$, is associated with the flow in the annulus. Note that $p_s$ = 0 for the quasi-static FDG case. $H$ is the hydrostatic head, and $l_{eff}$ is the effective length of the tube, allowing for all frictional losses in the tube.

The gauging nozzle was connected to a tube of true length, $l$ = 525 mm (apparatus 1) and $l$ = 393 mm (apparatus 2), with the other end open to the atmosphere. The value of the tube effective length, $l_{eff}$, used to account for frictional losses along the tube, fittings and in the bend, was a function of the tube Reynolds number. The value of $l_{eff}$ was determined from separate experiments employing a reservoir of stagnant liquid, and with the nozzle removed from the end of the tube, performed at clearances greater than 20 mm ($h/d_t$ » 2). The frictional loss along the siphon tube, $\Delta p_{34}$, was balanced by the hydrostatic head driving the flow. The value of $l_{eff}$ at different tube Reynolds numbers was determined using the Hagen-Poiseuille relationship; $l_{eff}$ was finally used to calculate $\Delta p_{34}$ in equation (2) when evaluating $C_d$.

**Numerical simulations**

CFD simulation was employed to model the quasi-static FDG and laminar flow FDG systems for apparatus 1 ($Re_{annulus} \leq 560$). Details of the quasi-static FDG simulation are reported in *Gu et al.* (2009a) in addition to results for laminar duct flow. The CFD computations were performed using the commercial FEM software, COMSOL MULTIPHYSICS™ (version 3.5, Chemical Engineering Module). All flows were laminar. The continuity and Navier-Stokes equations for a Newtonian liquid are:

Continuity: $$\nabla \cdot \mathbf{v} = 0 \qquad (3)$$

Navier-Stokes: $$\rho \mathrm{v} \cdot \nabla \mathbf{v} = -\nabla p + \mu \nabla^2 \mathbf{v} + \rho g \qquad (4)$$

where $\mathbf{v}$ is the velocity vector, $p$ the pressure, $\rho$ the density, $\mu$ the dynamic viscosity and $g$ the acceleration due to gravity, set to zero in this case for computational convenience (Tritton, 1988). Density and viscosity were set constant throughout the system.

**Boundary conditions**

A three dimensional model was set up illustrating a quarter of the annulus and half of the gauge, exploiting symmetry along the $y$-$z$ plane for the tube and both the $x$-$z$ and $y$-$z$ planes for the annulus (Fig. 4). The length of the annulus and the tube were shortened to reduce computing time. The liquid enters the system through the annulus base and leaves through the gauging tube and through the annulus top. The imposed boundary conditions were:

***(i) Annulus base* (z = 0)**

A mean $z$-wise velocity, $\overline{w}_{annulus}$ is specified at the annulus base, the value being taken from experiment. The $x$-wise and $y$-wise velocities $u$ and $v$ are set to zero at this plane.

***(ii) Annulus top, z = L'***

The length to diameter ratio, $L'/D_h$, was 3.6, determined via trial and error to be sufficient for the streamlines to be parallel at the top of the annulus. The pressure at the top is set to the (negative) gauge pressure, $p_s$, measured in experiment.

$$p_{1'} = -p_s \qquad (5)$$

***(iii) Gauging tube outlet, y = l'***

Fully developed flow is established, following the Hagen-Poiseuille velocity profile, *viz.*

$$v = v_{max}\left(1 - \left(\frac{2r}{d}\right)^2\right) \qquad (6)$$

where $r$ is the radial coordinate measured from the tube centre-line and $v_{max}$ is the maximum $y$-wise velocity, being twice the mean velocity calculated from experimental data. The $x$-wise and $z$-wise velocities $u$ and $w$ are set to zero. The length of the tube used in the simulations was $l'/d$ = 45, obtained by a numerical trial and error search for fully developed flow at the tube outlet.

***(iv) Walls***

The walls of the annulus, gauge, nozzle and the lip of the nozzle are all modelled as impermeable and non-slip.

***(v) Symmetry***

There is no flow across the $y$-$z$ and $x$-$z$ planes of symmetry, thus $\mathbf{n}\cdot\boldsymbol{v} = 0$, where $\mathbf{n}$ is the normal vector of the relevant plane.

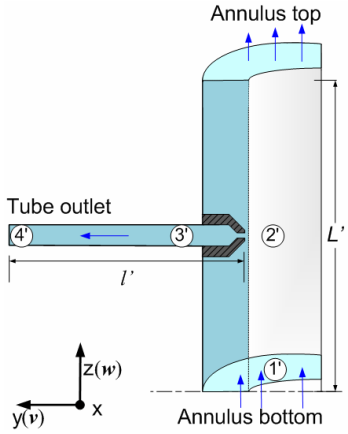


Fig. 4 Simulation geometry. Numbers refer to the stations in the simulation. The arrows indicate the entry flow in the annulus, and the exit flow in the tube and annulus top. Co-ordinates: $z$ – vertical (annulus) axis; $y$ – horizontal (gauging tube) axis. Velocity components $w$ and $v$ are indicated.

**Mesh**

The simulation domain was meshed with tetrahedral elements using the software's built-in mesh-generator. The size of the elements around the nozzle was smaller than the rest of the domain due to locally large velocity and pressure gradients in this region. The number of elements required to achieve convergence varied according to $h/d_t$, $Re_{tube}$ and $Re_{annulus}$.

To verify the accuracy of a particular solution, the number of elements ($N_e$) was varied (Table 1). The higher the number of mesh elements, the better the agreement between the $C_d$ experiment and simulation. Solutions took between 5 to 30 min to solve, using a desktop PC with a 2.61 GHz dual core processor and 3.25 GB RAM. Conservation of mass showed agreement to $10^{-5}$ kg/s or better for all cases investigated. This value was obtained by subtracting the annulus base (inlet) flow rate with the gauging tube (outlet) and annulus top (outlet) mass flow rates. In comparison, the smallest gauging tube mass flow rate was $4.8 \times 10^{-4}$ kg/s.

**Table 1: Mesh refinement result for the simulation case $h/d_t$ = 0.1, $Re_{annulus}$ = 90, $Re_{tube}$ = 150.**

| $N_e$ | $C_{d,\,sim}$ | $C_{d,\,exp}$ | % difference |
|---|---|---|---|
| 6124 | 0.259 | 0.258 | -0.49 |
| 5680 | 0.263 | | -2.07 |
| 4956 | 0.273 | | -5.81 |

## RESULTS AND DISCUSSION

**Calibration**

Fig. 5(a) shows a series of mass flow rate – clearance profiles for apparatus 1, spanning the range 90 ≤ $Re_{annulus}$ ≤ 29 000. The general increase in $m$ with $Re_{annulus}$ is related to the increase in $p_s$ with bulk flow rate. For laminar annular flows, the working range for the gauge, *i.e.* where $m$ is sensitive to $h/d_t$, lay between 0.06 to 0.30. It can be seen that as $Re_{annulus}$ increases, the working range extends to $h/d_t$ = 0.4 for $Re_{annulus}$ =29 000. These results are consistent with those of Gu *et al.* (2009a), where three zones of interest were identified, namely (*i*) *curvature*, (*ii*) *incremental* and (*iii*) *asymptotic*. The *curvature* zone arises from the presence of a curved surface. This can be clearly observed in Fig. 5(a), where $m$ never reaches zero because there will always be a gap for liquid to flow through between the flat nozzle tip and the curved substrate surface.

The increasing trend in mass flow rate – clearance profiles can also be observed in Fig. 5(b) for $Re_{annulus}$ 250 to 10 000 obtained using apparatus 2 and the 30° nozzle. The shape of the profiles was similar, *i.e.* increasing mass flow rate with clearance. The working range of apparatus 2 lay between 0.02 to 0.3 $h/d_t$. However, the curvature zone was smaller. This difference is attributed to the differences in the apparatus geometry. The diameter of the inner rod of apparatus 1 is almost twice that to apparatus 2 (21 mm *cf.* 12 mm), whilst the nozzle throat sizes are identical ($d_t$ = 1 mm). This means that with respect to the liquid near the nozzle throat, the geometry of apparatus 1 is more similar to that of a parallel plate when the nozzle is very close to the surface ($h/d_t$ < 0.04). For apparatus 2, for a given clearance the surface curvature is larger, allowing more liquid to flow and thereby reducing the extent of the curvature zone.

The difference between the two apparatuses and the two nozzles are compared. In Fig. 5(c) the characteristic mass flow rate – nozzle clearance profile is shown, where the discharge mass flow rate was divided by $m_\infty$ to yield a dimensionless profile. For the same clearance, more liquid flowed through gauge 2, due to a higher pressure driving force, a smaller nozzle rim, and a larger hydraulic diameter. The change in the nozzle geometry will also affect the mass flow rate, and this needs to be investigated separately. The Figure shows that the working range of the gauge for both nozzles lies in the range 0.06 < $h/d_t$ < 0.30.

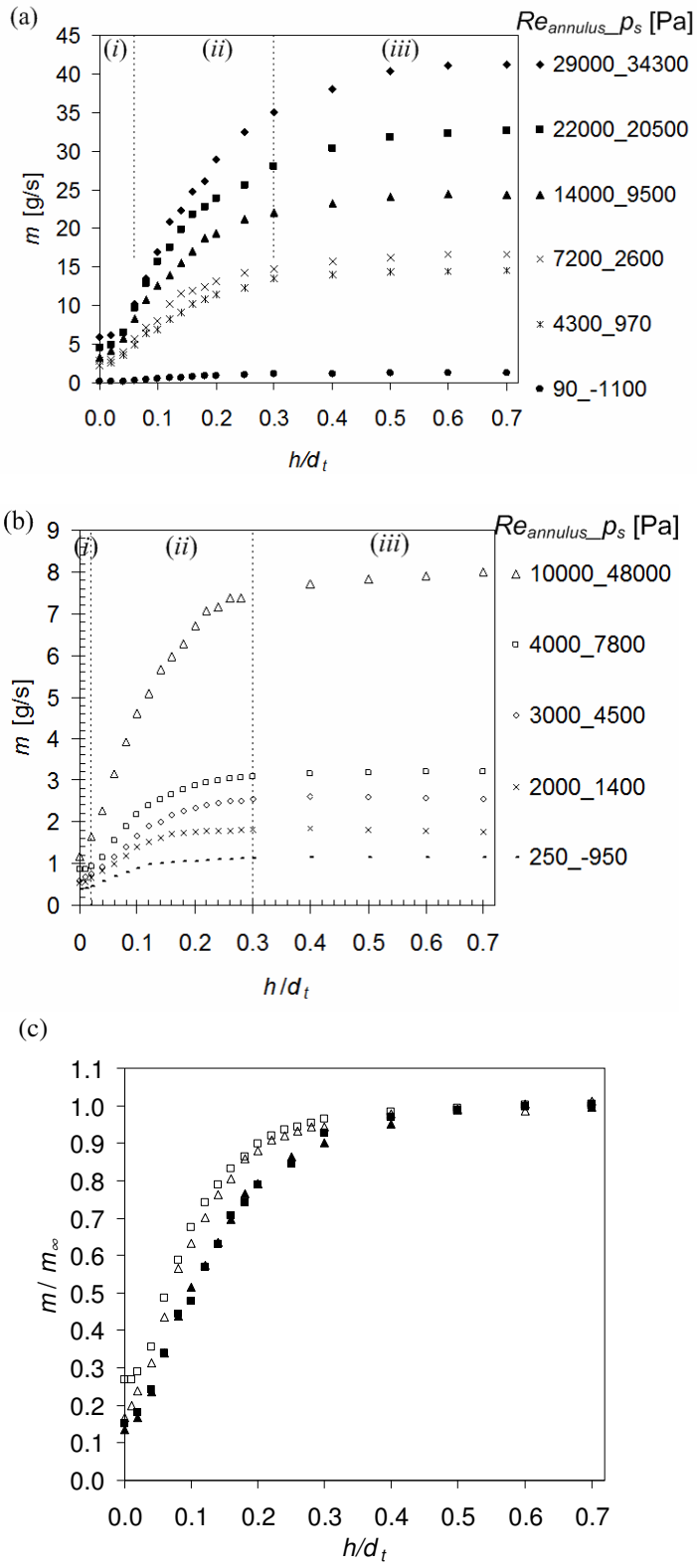


Fig. 5 Effect of $Re_{annulus}$ on experimental FDG mass profile. Regions marked: (*i*) *curvature* zone; (*ii*) *incremental* zone; (*iii*) *asymptotic* zone. (a) Apparatus 1, $\alpha = 45°$, $H = 405$ mm; (b) Apparatus 2, $\alpha = 30°$, $H = 350$ mm. (c) Data in (a) – solid symbols – and (b) – open symbols – plotted as dimensionless mass flow rate – clearance profiles.

**Discharge coefficient**

The effect of the geometry on the nozzle performance can be quantified via $C_d$. The effect of nozzle geometry on the asymptotic nozzle discharge coefficient, $C_{d,\infty}$, defined as the average value of $C_d$ at large clearances (e.g. $h/d_t \geq 0.6$), is shown in Fig. 6 for different values of $Re_{annulus}$. The 45° and 30° nozzles behaved quite differently; $C_{d,\infty}$ decreased slightly with increasing $Re_{annulus}$ for the 45° nozzle (apparatus 1), suggesting that the nozzle behaves less ideally at higher annular flow rates, whereas for the 30° nozzle the opposite trend was observed. The latter has a smaller angle and was also narrower, which is expected to reduce (*a*) the frictional losses underneath the rim, and (*b*) the disturbance to the flow in the annulus when the nozzle is far from the gauging surface. Both of these factors are hypothesized to contribute to lowering the hydraulic losses across the nozzle, giving larger values of $C_{d,\infty}$. For the lowest $Re_{annulus}$ values investigated, *i.e.* 90 and 250 for the 30 ° and 45 ° nozzle, respectively, both nozzles gave a common $C_{d,\infty}$ value of around 0.68.

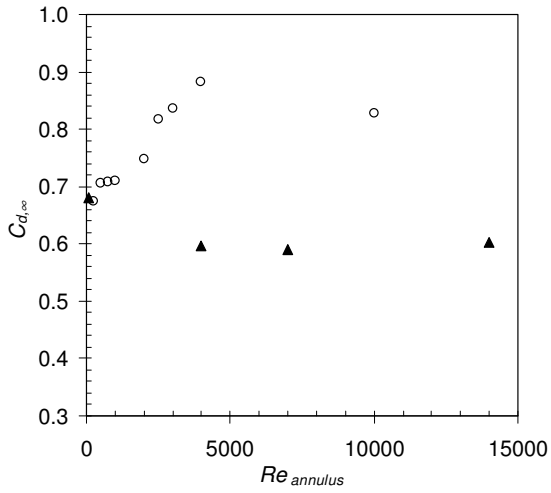


Fig. 6 Effect of $Re_{annulus}$ on asymptotic nozzle discharge coefficient $C_{d,\infty}$ for gauge 1 and 2, respectively. Symbols: solid triangles: gauge 1 (Fig. 1); open circles: gauge 2.

**Heated surfaces**

The effect of a heated surface on the discharge mass profile, studied using apparatus 2, proved to be negligible (Fig. 7). Wall temperatures were maintained at 20°C, 50°C, 80°C and 110°C for $Re_{annulus}$ values of 1700, 3000 and 10000, representing flows in the laminar, transitional and turbulent regime. The corresponding heat fluxes lay in the range 7-25 kW/m$^2$.

A slight increase in mass flow rate (6% or less) was noticed for the higher wall temperatures when the nozzle was located near the heated surface, due to the lower viscosity of the liquid in this region. Little difference was observed beyond 220 μm from the heated surface ($h/d_t$ = 0.22). These experiments were occasionally affected by bubble formation promoted by the hot surface, which affects the performance of the gauge.

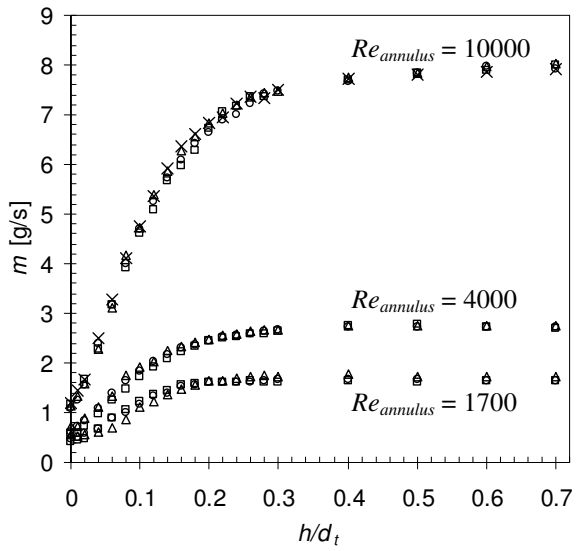


Fig.7 Apparatus 2. Effect of wall temperature on discharge mass flow rate. Bulk flow temperature 20 °C. Experimental conditions as in Fig. 5(b). Symbols: squares – 20 °C; circles – 50 °C; triangles – 80 °C; crosses – 110 °C.

For virtually all cases investigated, the mass flow rate through the gauge was only a fraction (less than or equal to 15%) of the total flow through the annulus. The exception is that for $Re_{annulus}$ = 90 (apparatus 1), where the maximum flow rate through the gauge approached 30% of the flow through the annulus inlet. This is unlikely to be desirable in a monitoring experiment.

**CFD simulation**

Table 2 summarises the results for a series of CFD simulations of FDG in (laminar) annular flow, for apparatus 1. The experimental and computed values of $C_d$ agreed to 10% or better for all cases. The simulated $C_d$ values lie for most cases within, or close to, the experimental $C_d$ error bars. For the range of $Re_{annulus}$ investigated, the agreement appears better for the lower $Re_{annulus}$ flows and for larger clearances ($h/d_t > 0.10$).

**Table 2: Summary of CFD simulation of FDG in annular flow [Apparatus 1].**

| $h/d_t$ | $Re_{annulus}$ | $C_{d,exp}$ | $C_{d,sim}$ | % diff. | $Re_{tube}$ |
|---|---|---|---|---|---|
| 0.10 | 560 | 0.266 | 0.240 | 10% | 542 |
| 0.14 | | 0.364 | 0.347 | 5% | 740 |
| 0.20 | | 0.481 | 0.473 | 2% | 973 |
| 0.10 | 300 | 0.261 | 0.240 | 8% | 532 |
| 0.14 | | 0.353 | 0.347 | 2% | 718 |
| 0.20 | | 0.476 | 0.472 | 1% | 964 |
| 0.10 | 190 | 0.264 | 0.240 | 9% | 538 |
| 0.14 | | 0.351 | 0.362 | -3% | 714 |
| 0.20 | | 0.472 | 0.472 | 0% | 956 |
| 0.10 | 90 | 0.258 | 0.240 | 7% | 527 |
| 0.14 | | 0.342 | 0.350 | -1% | 696 |
| 0.20 | | 0.465 | 0.472 | -2% | 941 |

The associated flow velocity distributions in the tube ($y$-direction) are presented in Fig. 8. The highest velocity occurs within the throat of the nozzle with expansion further along the tube. Asymmetrical flow in the tube is noticed when the gauge is close to the surface, at $h/d_t$ = 0.10, where the momentum from the annular flow is more influential, in agreement with results for square ducts reported by Gu *et al.* (2009b). The flow in the nozzle and tube becomes more symmetrical when the gauge is further away from the surface, *e.g.* $h/d_t \geq 0.14$.

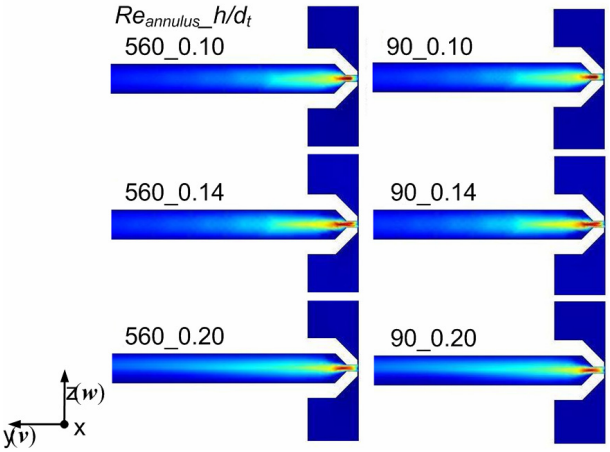


Fig. 8 Tube ($y$-wise) velocity component at the $y$-$z$ plane of symmetry for $Re_{annulus}$ of 560 and 90. Red colour indicates highest $y$-wise velocity and blue colour lowest value.

Values of shear stresses acting on the surface being gauged could be extracted from the CFD simulations. The surface is curved and hence the stresses acting on the surface along the annulus in the $z$-direction, and across the annulus in the $x$-direction, are different. Shear stress values are presented in Fig. 9(a) along the inner surface of the annulus in the $z$-direction, and in 9(b) along the arc length of the inner surface in the $x$-direction, for the simulation case $h/d_t$ = 0.10, 0.14 and 0.20, for $Re_{annulus}$ 550 and 90, respectively. The $z$-wise shear stress ($\tau_{yz'}$) is approximately zero at the centerline of the tube ($z'$= 0), reaches a maximum beneath the nozzle lip ($z'$ = 0.5 to 1.0 mm) and approaches zero asymptotically for $z' > 1$ mm. The magnitude of the $z$-wise shear stress at a given value of $z'$ decreases as the gauge is further away from the surface. The magnitude of these shear stresses is comparable with velocities used in cleaning-in-place operations (Timperley, 1989).

As the flow rate through the annulus increases, so does the shear stress underneath the gauging nozzle, but the dominant shear stress is that caused by the proximity of the gauge to the surface. When the gauge is close to the surface, *i.e.* at $h/d_t$ = 0.10, the shear stress is slightly higher upstream the gauge, which is an effect of the flow in the annulus.

The gap between the nozzle and the surface increases along the arc (Fig. 9(b)). The highest values of shear stress ($\tau_{za}$) occur within the throat and underneath the nozzle rim. The magnitude and shape of $\tau_{za}$ are similar to $\tau_{yz'}$ when the gauge is close to the surface, for $h/d_t$ of 0.10 and 0.14. However, when the nozzle is further away, at a clearance of

$h/d_t$ = 0.20, the shear stress $\tau_{za}$ exerted on a curved surface by the nozzle is less pronounced, which is why the shear stress decays from the centreline of the tube, rather than displaying peaks underneath the nozzle rim.

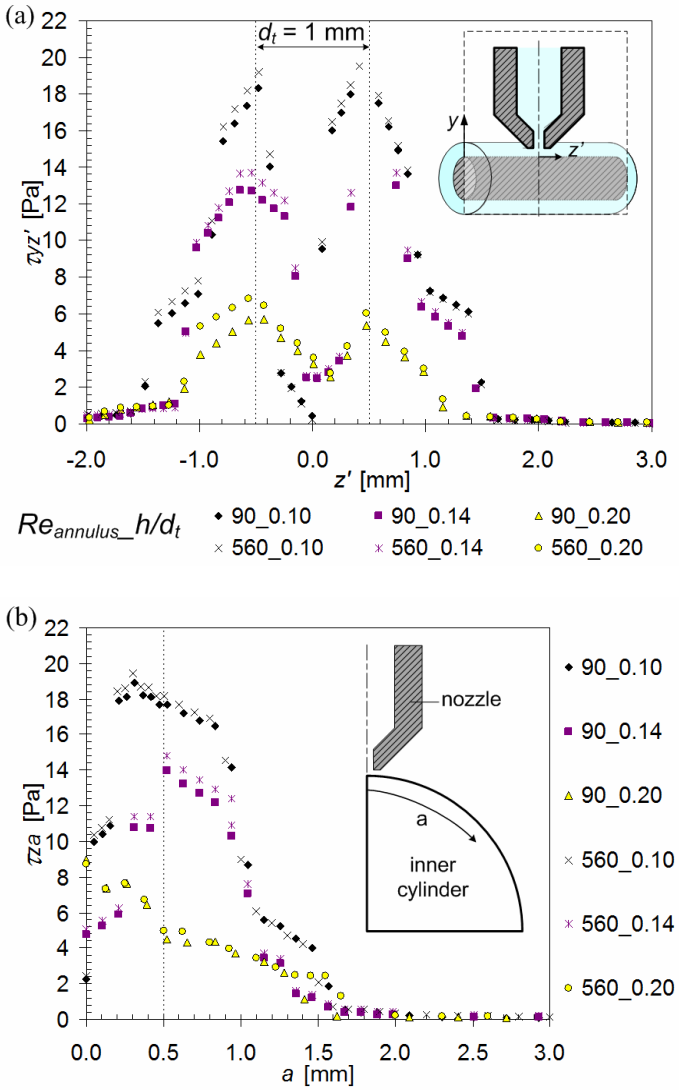


Fig. 9 Shear stresses imposed by the gauging flow on the inner surface of the annulus (*i.e.* at $y$ = 0), directly underneath the gauge, as illustrated in the inset. (a) Stress along the inner surface of the annulus in the $z'$-direction, $\tau_{yz'}$. (b) Shear stress, $\tau_{ya}$, imposed by the gauging flow on the inner surface of the annulus at different positions along the arc, $a$.

**Whey protein fouling**

5 wt% aqueous solutions of whey protein concentrate (WPC) was passed through apparatus 2 and allowed to run without interruption for 12 hr. The bulk temperature of the solution was maintained at 54 °C, the wall temperature at 95 °C, and a flow rate through the annulus of 0.22 m/s, corresponding to $Re_{annulus}$ = 7500. After 10 hr an increase in fouling resistance ($R_f$) was noticed, shown in Fig. 10, which indicated the formation of a fouling layer. The gauge measured a thickness of 200 µm. The layer was soft and gel-like, and was removed from the surface by the gauging flow (see inset in Fig. 10). Lumps of the deposit were observed in the discharge flow from the tube during the gauging experiment when the nozzle was close to the deposit surface. The layer dried quickly once the system had been drained. The nozzle left a ring of diameter 2 mm, in good agreement with the CFD predictions, suggesting that the dominant force of removal was caused by adhesive failure. To work out the shear stress and hence the forces of removal, a CFD model needs to be implemented incorporating the effect of heat transfer from the surface of the wall.

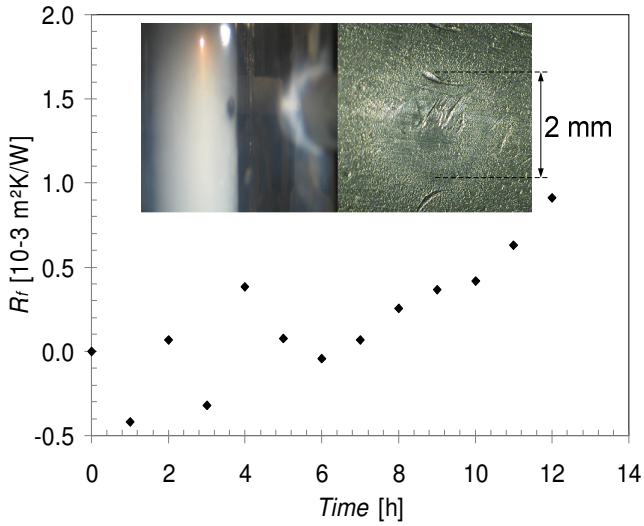


Fig. 10 Change in fouling resistance with time. Inset shows the image of the ring left by the nozzle.

## CONCLUSIONS

Fluid dynamic gauging has been successfully applied to laminar, transitional and turbulent annular flows for different annular geometries, and for a heated surface, at various wall temperatures. The practical working range of the gauge proved to be independent of the surface being heated. The gauge measured the thickness of a soft whey protein fouling layer *in situ*, and because of the proximity of the gauge to the surface, the soft deposit was removed by the forces of the gauging flow near the surface. CFD simulation demonstrated that the highest shear stresses are located under the rim of the nozzle, which was confirmed by the fouling experiment. To be able to predict the exact forces of removal of the deposit, further fouling experiments need to be performed.

## ACKNOWLEDGEMENTS

Funding for the Cambridge work from EPSRC (EP/D50306X), and a Research Fellowship for YMJC from the Royal Academy of Engineering, are gratefully acknowledged. This international collaboration was funded by the British Council and DAAD. The FDG apparatuses were constructed by Gary Chapman (Cambridge) and Karl Karrenführer (TU-BS).

## NOMENCLATURE

| | |
|---|---|
| $a$ | arc length along annulus cross section, m |
| $C_d$ | discharge coefficient, dimensionless |
| $d$ | inner diameter of dynamic gauging tube, m |
| $d_t$ | nozzle throat diameter, m |
| $D_h$ | hydraulic diameter of the annulus, m |
| $g$ | acceleration due to gravity, m/s$^2$ |
| $h$ | clearance between nozzle tip and gauging surface, m |
| $H$ | hydrostatic head providing pressure driving force for gauging flow, m |
| $k$ | wall thickness of gauging tube, m |
| $L'$ | CFD model duct length, m |
| $l$ | length of siphon tube, m |
| $l'$ | CFD model tube length, m |
| $m$ | tube discharge mass flow rate, kg/s |
| $\boldsymbol{n}$ | normal vector |
| $N$ | number |
| $p$ | pressure, Pa |
| $p_s$ | static pressure, Pa |
| $R_f$ | fouling resistance, m$^2$K/W |
| $Re$ | Reynolds number, dimensionless |
| $r$ | radial coordinate of the gauging nozzle, m |
| $s$ | width of nozzle rim, m |
| $u$ | $x$-wise velocity, m/s |
| $\mathbf{v}$ | velocity vector |
| $v$ | $y$-wise velocity, m/s |
| $\bar{v}$ | mean $y$-wise velocity, m/s |
| $w$ | $z$-wise velocity, m/s |
| $\bar{w}$ | mean $z$-wise velocity, m/s |
| $x, y, z$ | coordinates |

### Greek letters

| | |
|---|---|
| $\alpha$ | nozzle inner angle, ° |
| $\lambda$ | length of nozzle exit, m |
| $\mu$ | dynamic viscosity, Pa.s |
| $\rho$ | density, kg/m$^3$ |
| $\tau_{yz'}$ | shear stress on the $y$-plane in the $z$-direction, Pa |
| $\tau_{za}$ | shear stress on the $z$-plane in the $a$-direction, Pa |

### Subscript

| | |
|---|---|
| *actual* | actual |
| *annulus* | annulus |
| *e* | elements |
| *eff* | effective |
| *ideal* | ideal |
| *max* | max |
| *tube* | tube |
| *wall* | wall |
| ∞ | asymptotic |

### Acronyms

| | |
|---|---|
| CFD | computational fluid dynamics |
| FDG | fluid dynamic gauging |
| FEM | finite element method |
| TU-BS | technical university of Braunschweig |

## REFERENCES


Baker D.K., Vliet G.C., Lawler D.F., 1999, Experimental apparatus to investigate calcium carbonate scale growth rates, *Proc. of an International Conference on Mitigation of Heat Exchanger Fouling and its Economic and Environmental Implications*, Banff, Alberta, Canada.

Bennett C.A., Kistler R.S., Nangia K., Al-Ghawas W., Al-Hajji N., Al-Jemaz A, 2007, Observation of an isokinetic temperature and compensation effect for high temperature crude oil fouling, *ECI conference on heat exchanger fouling and cleaning*, Tomar, Portugal, Vol. RP5.

Gu T., Chew Y.M.J., Paterson W.R., Wilson D.I., 2009a, Experimental and CFD studies of fluid dynamic gauging in annular flows, *AIChE Journal*, in press.

Gu T., Chew Y.M.J., Paterson W.R., Wilson D.I.. Experimental and CFD studies of fluid dynamic gauging in duct flows, 2009b, *Chemical Engineering Science*, Vol. 64, Issue 2, pp. 219-227.

Hooper R.J., Liu, W., Fryer, P.J., Paterson, W.R., Wilson, D.I. Zhang, Z, 2006, Comparative studies of fluid dynamic gauging and a micromanipulation probe for strength measurements, *Food & Bioproducts Processing*, Vol. 84, pp. 353-358.

Timperley, D.A., 1989, Cleaning in place, Journal of Dairy Technology, Vol. 42, Issue 2, pp. 32-33.

Tritton, D.J., *Physical Fluid Dynamics* (2nd edition), 1988, UK Oxford University Press, , pp. 58–59.

Tuladhar T.R., Macleod N, Paterson W.R., Wilson D.I., 2000, Development of a novel non-contact proximity gauge for thickness measurement of soft deposits and its application in fouling studies, *Canadian Journal of Chemical Engineering*, Vol. 78, pp. 925-947.

Tuladhar T.R., Paterson W.R., Wilson D.I., 2003, Dynamic gauging in duct flows, *Canadian Journal of Chemical Engineering*, Vol. 81, pp. 279-284.